Journal of the Civil Engineering Forum, May 2025, 11(2):113-124
DOI 10.22146/jcef.15085
Available Online at https://jurnal.ugm.ac.id/v3/jcef/issue/archive

Numerical Study of Wave Reflection by The Curtain Wall-Pile Breakwater Using the SPH Model

Muhammad Farizqi Khaldirian[1*], Marcio Tahalele[2], Inggrit Tri Rida Wahyu Satiti[3]
[1]Department of Civil and Environmental Engineering, Universitas Gadjah Mada, Yogyakarta, INDONESIA
[2]Civil Engineering Program, Soegijapranata Catholic University, Semarang, INDONESIA
[3]Department of Civil and Environmental Engineering, Imperial College London, London, UNITED KINGDOM
*Corresponding author: muhammad.farizqi.k@ugm.ac.id

SUBMITTED 23 July 2024 **REVISED** 2 December 2024 **ACCEPTED** 3 December 2024

ABSTRACT The Curtain Wall-Pile Breakwater (CPB) is comprised of a precast concrete wall structure that is upheld by pillars. The effectiveness of this breakwater has been extensively examined through experimental and numerical approaches in comparison to the conventional gravitational breakwater due to its reduced underwater footprint, which could be more environmentally sustainable. A Smoothed Particle Hydrodynamics (SPH) model using the open-source algorithm DualSPHysics is presented in this paper to simulate wave reflection on a CPB for multiple variables. This study focused on assessing the CPB's performance in reflecting wave energy represented by the reflection coefficient (C_r), with a detailed investigation of two key parameters: relative depth, which is the ratio of wall depth to water depth (h/d) and wave steepness (H_i/L). The physical model was also tested in a laboratory flume to confirm the accuracy of the simulation results obtained through SPH. A fluid particle size of 0.5 cm was used, resulting in a simulation comprising approximately 9,320,717 particles. The results indicate that the Cr is directly proportional to the h/d and significantly influenced by H_i/L. Specifically, changes in h/d from 0.0 to 0.7 resulted in Cr increases from approximately 0.21 to 0.49 for lower wave steepness (H_i/L = 0.0097) and from approximately 0.36 to 0.60 for higher wave steepness (H_i/L = 0.0499). The quantitative analysis based on the quadratic regression equations shows that both the relative depth and wave steepness significantly influence the effectiveness of the CPB. The reflection coefficient increases with the relative depth, with a more significant effect observed for higher wave steepness. These findings underline the importance of considering both parameters in the design and optimization of breakwater structures to ensure robust and effective coastal protection.

KEYWORDS Curtain Wall-Pile, Wave Reflection, Reflection Coefficient, Smoothed Particle Hydrodynamics

1 INTRODUCTION

Gravity-type breakwaters are widely used to protect shorelines and maintain calm conditions in harbor anchorage areas. However, their effectiveness decreases in deeper waters, as they require significantly more space and materials, making them less sustainable and more harmful to the marine environment. To address these limitations, the Curtain Wall-Pile Breakwater (CPB) has been introduced as a more environmentally friendly alternative. This permeable breakwater design minimizes seabed intervention by utilizing a pile-supported vertical wall arrangement, reducing ecological impact while maintaining functionality (Suh et al., 2007; Rao et al., 2019). This breakwater design is considered permeable due to the gaps between the piles, which vary depending on the wall's underwater depth. This enables the preservation of the beach's natural physical processes by minimizing disturbance to the movement of particles, allowing them to pass through the breakwater and may prevent issues like erosion and siltation (Laju et al., 2005).

Transmission waves passing through a breakwater are a crucial factor in breakwater design, and the efficiency of breakwater energy dissipation can be assessed by considering its correlation with wave reflection. Some waves split from the incident wave, partly being reflected as reflection waves and some passing through the permeable breakwater structure (Vu et al., 2022). Despite the ecological advantages of CPBs, there remain open questions regarding their effectiveness in dissipating wave energy, particularly under varied wave and structural conditions. The role of reflection coefficients under different structural and wave parameters is yet to be fully explored.

Wibowo et al. (2020) performed a two-dimensional physical model in a wave flume to investigate the correlation between reflection coefficient, transmission coefficient, and structural variables on the Single Chamber Skirt Breakwater (SCSB). Research findings indicate that peak performance (50% effectiveness or Cr = 0.5) is achieved at intermediate depths ranging from 1.5 > k_h > 2.0. Suh et al. (2006) developed a mathematical model to examine the rectangular pile and then adapted the model for the circular pile (Suh et al., 2007). The comparison between measurement and pre-

diction indicates that the mathematical model effectively replicates the key aspects of the experimental results. However, the reflection coefficients were overpredicted for larger wave heights, contradicting the linear wave theory. Subekti and Shulhany (2021) conducted a physical modelling study of the CPB, analyzing various dimensionless variables to determine their impact on the reflection coefficient. The reflection coefficient is directly proportional to the ratio of the wall's relative depth to the water depth, and this proportionality similarly extends to the wave steepness. Additionally, an empirical reflection coefficient equation is derived from a subset of the relationship data using the variables, in the structure of a multivariable linear equation. While previous research provides valuable insights into wave interaction with breakwater structure including CPBs, there is a need for further studies to explore wave reflection and energy dissipation using advanced numerical methods and more comprehensive models.

Smoothed Particle Hydrodynamics (SPH) is a Lagrangian particle method that has advanced significantly in the past twenty years. It is highly reliable for simulating intricate hydraulic and coastal engineering issues due to its capability to handle significant deformation, flows dominated by advection, and problems involving multiple phases. Thus, it shows potential for accurately replicating the natural fluid behavior (Luo et al., 2021). The Lagrangian motion description involves tracking individual particles of a continuum as they move through space and time. This approach treats particles as distinct entities and monitors the trajectory of each individual particle. The convective component can be removed from the governing equation without the need for numerical stability. The Lagrangian particle retains data on variables that have undergone changes in the past during the deformation process. The variables' values change based on the particle's previous state and interactions with neighboring particles, which also affect the particle (Khaldirian et al., 2021). Given the complex interactions between waves and permeable breakwaters, SPH offers a promising approach for modeling wave reflection, transmission, and dissipation, areas which have not been fully addressed in prior CPB studies.

DualSPHysics is one of the SPH algorithms that utilizes the C++ programming language and hardware with GPUs supported by CUDA for computing. Aside from the DualSPHysics code-based Computational Fluid Dynamics (CFD) application, software like SketchUp, Notepad++, ParaView, and Blender can also be utilized for conducting simulations in this research (Tahalele et al., 2022). Pawitan et al. (2024) conducted an experiment to analyze how waves affect elevated structures with vertical and inclined walls using the open-source SPH algorithm, specifically DualSPHysics. The study revealed that the height of the structure above the water surface influenced the pressure exerted on the structure when the wave broke. The results were effectively correlated with the experimental tests conducted. However, challenges may arise when modeling on a large scale, necessitating a substantial number of particles due to the Lagrangian nature of SPH. Fourtakas and Rogers (2016) enhanced the open-source DualSPHysics software to speed up SPH simulations on multiphase models with millions of particles through the implementation of GPU parallelization methods. This technique accelerates 58 times faster over a significantly larger modelling domain while maintaining accuracy with experimental data.

Despite these advancements, the application of SPH to CPB studies remains limited. While CPBs have been examined extensively through physical modeling and empirical approaches, these previous studies remain open for further investigate the intricate dynamics of wave reflection and transmission under varied conditions. Therefore, this study employs DualSPHysics to fill this gap, focusing on the numerical assessment of CPB performance, particularly in terms of wave reflection behavior under different wave steepness and structural configurations.

2 METHODS

2.1 SPH Formulation

The SPH is a meshless Lagrangian technique that represents continuous fluids as discrete particles. The particles contain fluid parameters that are utilized to analyze physical characteristics (such as position, direction, and magnitude) according to the Navier-Stokes equations. The interaction between particles in both two and three dimensions is determined by the kernel function (W) within a specific boundary smoothing length (h). The fluid variable F at position r is calculated for each timestep by considering the variable of its neighboring particles at position r'.

$$F(r) = \int F(r')W(r - r', h)dr \tag{1}$$

Alternatively, in discrete form

$$F(r_a) \approx \sum\nolimits_b F(r_b)\frac{m_b}{\rho_b}W(r_a - r_b, h) \tag{2}$$

a and b represent individual particles. m_b and ρ_b represent the mass and density of the particle, respectively. The kernel function is defined as a function of the non-dimensional distance between particles, denoted as $q = r/h$, where r represents the distance between particles a and b. The smoothing length parameter h determines the radius of the region surrounding particle where in-

fluences from other particles are significant. The kernel function utilized is Quintic according to Wendland (1995), defined by the following equation.

$$W(q) = a_d \left(1 - \frac{q}{2}\right)^4 (2q+1) \text{ for } 0 \le q \le 2 \tag{3}$$

where $a_d = 7/4\pi h^2$. The momentum equation for particle a with respect to particle b is derived from the equations 1 and 2 as follows (Monaghan, 1994).

$$\frac{dv_a}{dt} = -\sum\nolimits_b m_b \left(\frac{P_b + P_a}{\rho_b \rho_q} + \Pi_{ab}\right) \nabla_a W_{ab} + g \tag{4}$$

where g represents the gravitational acceleration, P is the pressure calculated at particle a or b, W_{ab} is the kernel function between particles a and b, and the artificial viscosity term Π is defined as

$$\Pi_{ab} = \begin{cases} \dfrac{-\alpha \overline{C_{ab}} \mu_{ab}}{\overline{\rho_{ab}}} & \text{for } v_{ab} \cdot r_{ab} < 0 \\ 0 & \text{for } v_{ab} \cdot r_{ab} \ge 0 \end{cases} \tag{5}$$

$$\overline{\rho_{ab}} = 0.5(\rho_a + \rho_b) \tag{6}$$

$$r_{ab} = r_a - r_b \tag{7}$$

$$v_{ab} = v_a - v_b \tag{8}$$

$$\mu_{ab} = \frac{h v_{ab} \cdot r_{ab}}{r_{ab}^2 + \eta^2} \tag{9}$$

$$\overline{C_{ab}} = 0.5(c_a + c_b) \tag{10}$$

$$\eta^2 = 0.01 h^2 \tag{11}$$

The velocity of the particle is represented by v, the speed of sound by c, the distance between particles a and b by r_{ab}, and α denotes the dissipation coefficient in the artificial viscosity term, which is fixed at 0.01 since it is the minimum value is necessary to provide stability in the numerical scheme (Reis et al., 2022; Altomare et al., 2015; Barreiro et al., 2013). The variation in fluid density over time is calculated using the continuity equation.

$$\frac{d\rho_a}{dt} = -\sum\nolimits_b m_b v_{ab} \nabla_a W_{ab} \tag{12}$$

SPH treats the fluid as weakly compressible, allowing for extremely small changes in density similar approximately as incompressible fluids. Following Monaghan (1994) and Batchelor (1999), this enables the use of the equation of state to study the relationship between density and pressure as follows.

$$P = B\left[\left(\frac{\rho}{\rho_0}\right) - 1\right] \tag{13}$$

where γ = 7 and $B = c_0^2 \rho_0 / \gamma$, with ρ_0 = 1000 kg m^{-3} (the reference density) and $c_0 = c(\rho_0) = \sqrt{\partial P / \partial \rho}\Big|_{\rho_0}$ (the speed of sound at the reference density).

The time step in SPH is determined by fluid properties due to its impact on velocity magnitude. Increasing velocity leads to faster changes in position, requiring adjustment of the time step (Δt) to maintain numerical stability. The timestep is typically determined by the Courant-Friedrich-Lewy (CFL) condition, viscous diffusion term, and forcing term from the following equations.

$$\begin{aligned} \Delta t_f &= CFL \cdot \min\left(\Delta t_f, \Delta t_{CV}\right) \\ \Delta t_f &= \min_a \left(\sqrt{\frac{h}{|f_a|}}\right); \\ \Delta t_{cv} &= \min_a \frac{h}{c_s + \max_a |h v_{ab} r_{ab} / \left(r_{ab}^2 + \eta^2\right)|}; \end{aligned} \tag{14}$$

where Δt_f represents force per unit mass $(|f_a|)$, and Δt_{cv} represents combination of Courant and viscosity control.

2.2 Boundary Conditions

This simulation utilizes a dynamic boundary condition (DBC). DBC enforces boundary particles (CPB model and flume) that follow the same equation as fluid particles but remain in a stationary state. When fluid particles approach boundary particles within a distance less than twice the smoothing length (h), the density of boundaries increases, leading to a rise in pressure, with fixed boundary conditions, then based on the momentum equation, there is a repulsive force that drives the fluid particles (Crespo et al., 2015). Specifically, for wave makers that move with a particular motion pattern, DBC is also enforced. However, the motion is determined by an external function that is prescribed and desired, rather than by the governing equation applied.

2.3 Wave Generation

As described in sub-section 2.2, waves are produced through fluid interaction with the wave maker utilizing a flap. The motion attributed to this wave generator acts as the moving boundary that generates the wave, which is then governed by the governing equations, whereas the moving boundary is independent of the fluid movement. The second-order wave component is produced because of the motion of the first-order wave maker and the free surface boundary conditions, which include inhomogeneous terms that depend on the first-order solution (Aghaei et al., 2021). According to Madsen (1971), second-order wave equations are provided,

producing progressive, relatively long waves with a more peaked crest. This second-order wave theory is then implemented into DualSPHysics to express the flap motion equation on the wave maker (Domínguez et al., 2021).

$$X(t) = \frac{H}{2m_{cr}} \sin\left(\frac{2\pi t}{T} + \varphi\right) + \left[\left(\frac{H^2}{32\left(1 - \frac{d}{2(d+d_0)}\right)}\right) \cdot \left(\frac{3\cosh\left(\frac{2\pi d}{L}\right)}{\sinh^3\left(\frac{2\pi d}{L}\right)} - \frac{2}{m_{cr}}\right)\right] \sin\left(\frac{4\pi t}{T} + 2\varphi\right) \tag{15}$$

where m_{cr} is given by

$$m_{cr} = \frac{4\sinh\left(\frac{2\pi d}{L}\right)}{\sinh\left(\frac{2\pi d}{L}\right) + \frac{2\pi d}{L}} \cdot \left[\sinh\left(\frac{2\pi d}{L}\right) + \frac{1 - \cosh\left(\frac{2\pi d}{L}\right)}{\frac{2\pi}{L}(d + d_0)}\right] \tag{16}$$

where H is the wave height $\varphi[0, 2\pi]$ is the initial phase, d is the water depth, d_0 is the depth of hinge location ($d_0 = 0$, as hinge is on the bottom), $2\pi/T$ is the angular frequency, $2\pi/L$ is the wave number, T is the wave period, and $X(t)$ is the flap-type wave maker displacement at the free surface.

2.4 Wave Reflection

Studying wave reflection is crucial when designing coastal structures, particularly in port regions. The coastal area protected by a coastal structure will experience reduced noise as the waves passing through it decrease in size. To reduce the transmission of waves, structures that effectively reflect the waves should be used. When a wave encounters a structure, it will be reflected by the structure. A wave exhibiting perfect reflection results in a standing wave with a wave height in front of the barrier that is double the height of the incoming wave. If the barrier has porosity, gaps, or imperfect reflection, the wave height in front of the barrier will be less than twice the height of the incident wave, leading to a partial standing wave (Dean and A, 1984). When a wave undergoes incomplete reflection and encounters an obstacle, the height of the incident wave (Hi) will exceed that of the reflected wave. The incident and reflected waves have identical periods, resulting in wavelengths that are equal but traveling in opposite directions. The wave profile approaching the barrier before impact is represented by the equation.

$$\eta_i = \frac{H_i}{2} \cos(kx - \sigma t) \tag{17}$$

The reflection wave profile caused b the incident wave hitting the barrier can be represented as

$$\eta_r = X\frac{H_i}{2} \cos(kx - \sigma t) \tag{18}$$

where $0 \leq X \leq 1$. The wave profile in front of the barrier after the wave hits the model is the combination of equations 17 and 18 represented by the formula.

$$\eta = \eta_i + \eta_r = \frac{H_i}{2} \cos(kx - \sigma t) + X\frac{H_i}{2} \cos(kx - \sigma t) \tag{19}$$

$$\eta = (1 - X)\frac{H_i}{2} \cos(kx - \sigma t) \tag{20}$$

where k is the wave number, σ is the frequency, η_i is the incident wave profile, η_r is the reflected wave profile and η is the superposition of the incident and reflected wave. Imperfect reflection results in the absence of real nodes in the wave profile instead there will be a small oscillation forming a minimum amplitude $(a_{\min})$ of partially standing wave located at one quarter of the wavelength from the point of maximum amplitude $(a_{\max})$ in the oscillation as shown in Figure 1.

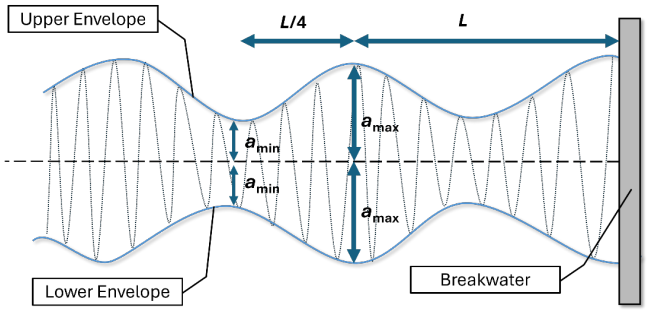

Figure 1 Partially standing waves

For vertical impermeable walls, the reflection coefficient is approximately 1, resulting in a reflected wave height equal to the incident wave. If there is a perfect reflection, $X = 1$, Thus, the wave profile equation is written as follows:

$$\eta = H_i \cos kx \cos \sigma t \tag{21}$$

The equation indicates the fluctuation of the surface of the water in the standing wave (clapotis) which is periodic to time (t) and to distance (x). when $\cos kx = \cos t = 1$, then the maximum height is $2H_i$. This indicates that the wave height in front of the vertical structure can reach a maximum height of twice the incident waves.

The superposition of two waves with equal periods and opposite directions, each with amplitudes a_1 and a_2, is described by the following equation.

$$\eta = a_1 \cos(kx - \sigma t) + a_2 \cos(kx - \sigma t) \tag{22}$$

The equation above represents the imperfect reflective wave, where a_1 is the amplitude of the incident wave and a_2 is the amplitude of the reflected wave. The a_{max} is the sum of a_1 and a_2, while the a_{min} are the difference of a_2 and a_1. The reflected wave height (H_r) is defined as half the difference between the maximum wave heights (H_{max}) and the minimum wave heights (H_{min}), or equivalently as the fluctuation derived from twice the wave amplitudes.

$$H_r = \frac{2a_{\text{max}} - 2a_{\text{min}}}{2} = \frac{H_{\text{max}} - H_{\text{min}}}{2} \tag{23}$$

The structure's capacity to reflect a wave is determined by the reflection coefficient (C_r), which is calculated as the ratio of the reflected wave height to the incident wave height (H_r/H_i).

$$C_r = \frac{a_2}{a_1} = \frac{a_{\text{max}} - a_{\text{min}}}{a_{\text{max}} + a_{\text{min}}} = \frac{H_{\text{max}} - H_{\text{min}}}{H_{\text{max}} + H_{\text{min}}} \tag{24}$$

$$C_r = \frac{H_r}{H_i} \tag{25}$$

2.5 Model Parameters

The variations of the parameters applied to the model are non-dimensional parameters as shown in Table 1. The parameter associated with the CPB permeability is based on several scenarios of the depth of the curtain wall relative to the water depth (h/d) under two incident wave characteristic conditions represented by the wave steepness or the ratio between wave height and wavelength (H_i/L). The wave steepness values are chosen based on the wave parameter values derived from laboratory measurements of the generated wave since the parameter values are not set but converted from wave generator settings.

2.6 Model Validation

The model was validated by comparing the surface fluctuations of waves in the SPH simulation with the experimental results. The wave experiments, specifically conducted for this study, were carried out at the Coastal Engineering and Hydraulics Laboratory of PAU Universitas Gadjah Mada. The 18-meter-long flume with a width of 30 cm and a water depth of 20 cm was utilized. The initial validation was conducted in the absence of the breakwater model installed in the flume.

Table 1. Variation of modelling parameters

Wave Period (T) (s)	Incident Wave Height (Hi) (mm)	Wavelength (L) (m)	H_i/L	h/d
2.0313	26.71	2.7536	0.0097	0.0
2.0313	26.71	2.7536	0.0097	0.1
2.0313	26.71	2.7536	0.0097	0.3
2.0313	26.71	2.7536	0.0097	0.5
2.0313	26.71	2.7536	0.0097	0.7
0.9347	55.36	1.1083	0.04995	0.0
0.9347	55.36	1.1083	0.04995	0.1
0.9347	55.36	1.1083	0.04995	0.3
0.9347	55.36	1.1083	0.04995	0.5
0.9347	55.36	1.1083	0.04995	0.7

A comparison of wave fluctuations was conducted during the early stage of wave generation to compare the incident wave in its pure form with the experimental wave prior to the occurrence of reverse reflection. However, the SPH model does not include a wave damper, whereas the experimental setup utilized a wave damper at the end of the flume. The exact damping rate of the wave damper used in the experiment was not measured, which represents a limitation in aligning the two models. A wave probe (WP) was positioned a considerable distance in front of the model to measure the incident waves generated by the wave maker.

Another validation was performed to compare the wave fluctuations at the moment after the reflection occurred in front of the model. The breakwater model was positioned 9 meters away from the wave maker in the flume. WP1 was positioned in front of the breakwater model at about 1 wavelength (1*L*) to capture the water fluctuation at the point of highest amplitude. WP2 was positioned 1.25 wavelength (1.25*L*) away to measure water surface when the minimum fluctuation occurs. The specific distance values are provided in Table 2. Additionally, WP3 was located 3.75 meters from the wave maker to ensure accurate measurement of the incident wave profile.

Table 2. Distances of Wave Probes (WP1 and WP2) from the CPB Structure for Different Wave Steepness Values (H_i/L)

H_i/L	WP1 (1*L*) (m)	WP2 (1,25*L*) (m)
0.0097	2.75	3.44
0.04995	1.10	1.38

Figures 3 illustrates a comparison between SPH results and experimental data for incident wave fluctuations without a breakwater and wave fluctuations in front of a breakwater model. Figure 3(a) and Figure 3(b)

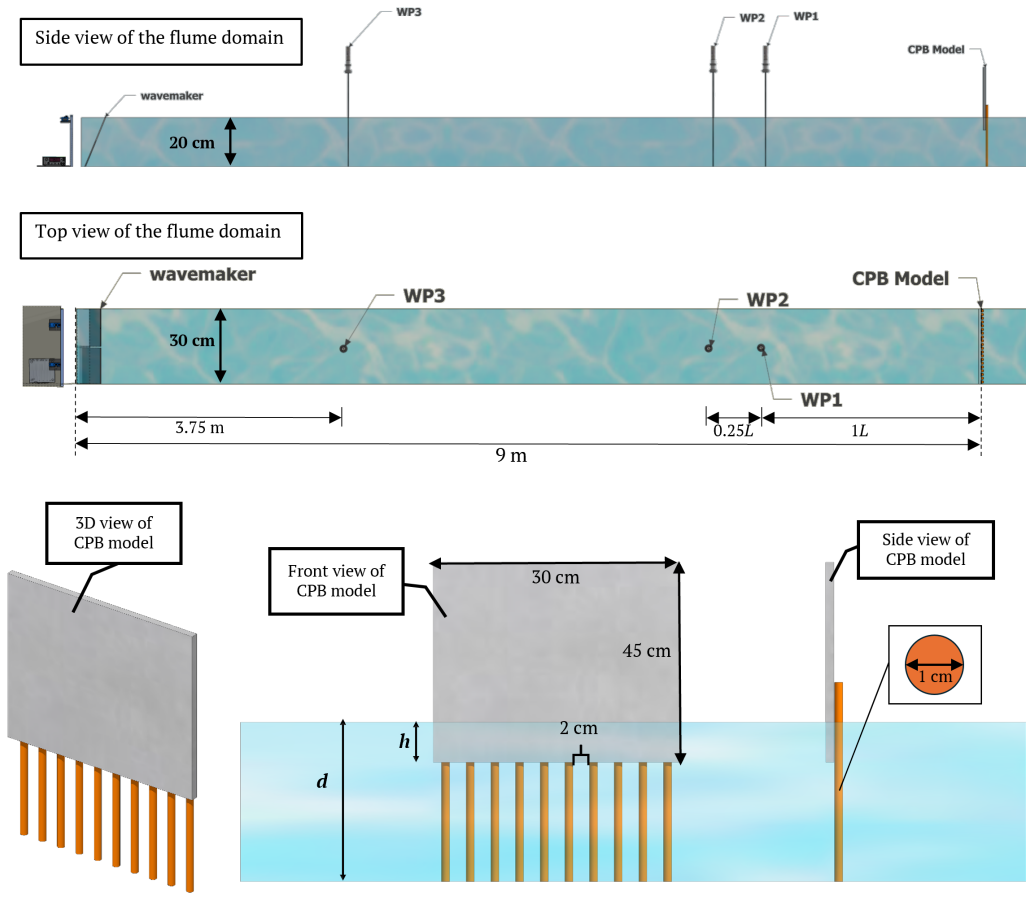

Figure 2 Experimental setup of the flume domain and the CPB model, representing the physical model configuration.

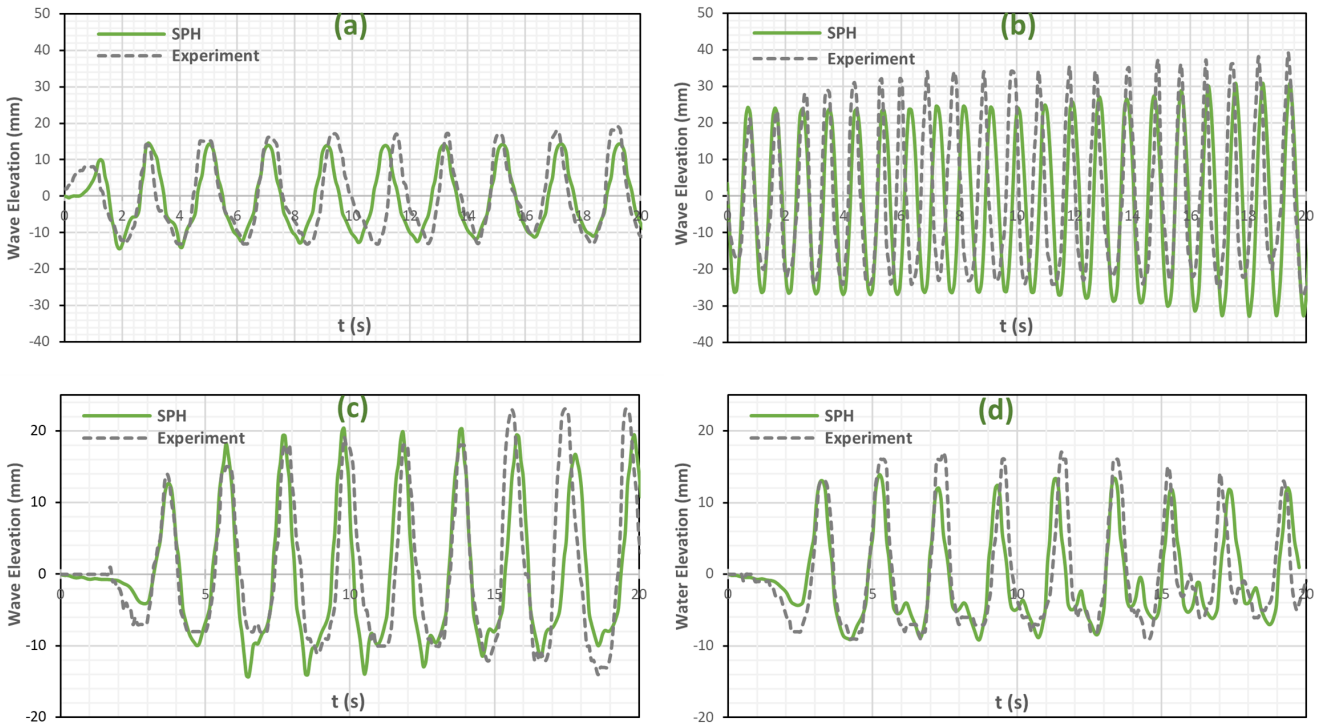

Figure 3 Comparison of SPH simulations and experimental data. Graphs **(a)** and **(b)** show incident wave fluctuations without a breakwater for H_i/L = 9.70E-03 and H_i/L = 4.99E-02, respectively. Graphs **(c)** and **(d)** present maximum and minimum wave fluctuations in front of a breakwater.

compare numerical and experimental results for wave fluctuations without a breakwater structure at different wave steepness values (H_i/L = 0.0097 and H_i/L = 0.0499, respectively). In both cases, the SPH model demonstrates better accuracy during the earlier phase of the wave fluctuations, closely capturing both the amplitude and phase. This suggests that the SPH model effectively represents the wave dynamics when conditions are still developing, prior to secondary effects such as wave re-reflection or dissipation. Figure 3(c) and Figure 3(d) present comparisons for maximum and minimum wave fluctuations, respectively, in front of a breakwater model. The SPH model follows the experimental results closely, with a relatively robust correlation in amplitude and phase for both the maximum and minimum wave elevations. Notably, the model's performance is most accurate during the initial wave-CPB interaction phase, which is critical for evaluating the pure reflection caused by the CPB structure. While the SPH model shows good agreement with experimental results, some errors are expected due to limitations in the numerical model and experimental factors. These include differences in boundary conditions treatment that may not perfectly replicate physical experiments such as the absence of wave absorbers in the numerical model. Resolution and particle size also affect how accurate wave interactions could be accurate, specifically for phenomena such as turbulence, wave breaking, and interactions with structures. Experimental errors and noise, as well as complex physical processes like turbulence and viscosity, might also contribute to the discrepancies.

3 RESULTS AND DISCUSSIONS

In this section, the effect of wave characteristics and the submerged wall depth relative to the water depth on wave reflection are studied. The geometry of the CPB is illustrated in Figure 2. A 1/60 scale model prototype was designed based on Froude similitude. The SPH model used in this study employs a fluid particle size of 0.5 cm, which ensures a fine resolution necessary for capturing the detailed interactions between the fluid and the breakwater structure. This granularity is crucial for accurately simulating wave behavior and its interaction with the CPB. The total number of particles used in the simulation was approximately 9,320,717, allowing for a high degree of detail and precision in the results. This model comprises two main components, a vertical curtain wall and a pile foundation. The curtain wall acts as the primary barrier to incoming waves, extending both above and below the water surface to effectively reduce wave energy and impact. The piles, depicted as vertical elements driven into the seabed, provide structural support and stability to the curtain wall, preventing displacement due to wave forces. The model highlights key depth parameters: the depth of the curtain wall below the water surface, and the water depth from the surface to the bottom. These parameters are crucial for determining the breakwater's placement and design. The CPB used in the model is a vertical wall positioned in front of an arrangement of circular piles (see Figure 2). The dimensions of the curtain wall are 30 cm wide (the same width as the flume) and 45 cm high to allow the position of the wall to be adjusted. The curtain wall is designed to have a thickness of 1 cm, which

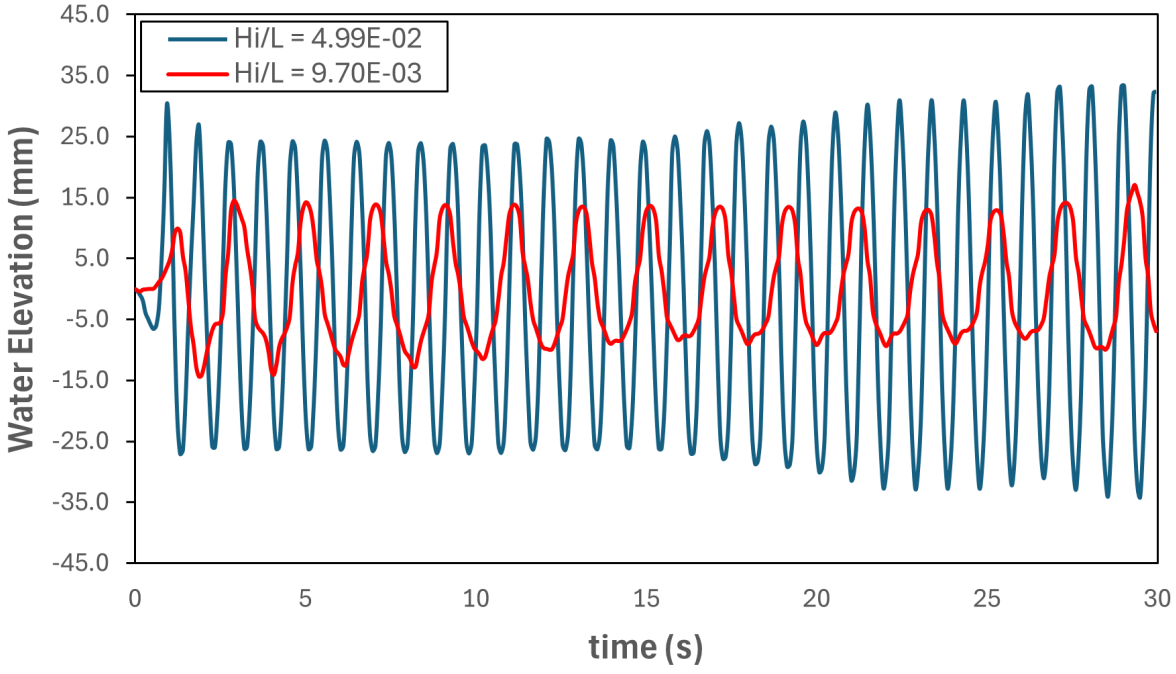

Figure 4 Incident wave fluctuation over time for different wave steepness. The plot shows water elevation (mm) versus time (s) for two wave steepness: H_i/L = 4.99×10-2 and H_i/L = 9.7×10-3, illustrating the difference in wave frequency and amplitude.

is similar to the diameter of the piles.

A time series of incident wave fluctuations in Figure 4, illustrating the effect of different wave steepness on water fluctuation over time. The plot compares two wave steepness scenarios, H_i/L = 4.99×10^{-2} (blue line) and H_i/L = 9.7×10^{-3} (red line). The data show distinct differences in wave frequency and amplitude between the two steepness values. For H_i/L = 4.99×10^{-2}, the waves exhibit higher frequency and larger amplitude fluctuations, reflecting more energetic wave conditions. In contrast, the waves with H_i/L = 9.7×10^{-3} show lower frequency and smaller amplitude, indicating less energetic wave conditions. This comparison underlines the significant impact of wave steepness on wave dynamics, with higher steepness resulting in more pronounced wave fluctuation. Figure 5 presents wave reflection patterns at different wave steepness and relative depth, captured at an early stage of the reflection process to ensure that the reflected waves are formed purely by the interaction with the breakwater and isolating it from potential complications that may arise in later stages, such as re-reflection effects. As h/d increases (from 0.1 to 0.7), the interaction between the wave and the structure grows stronger, resulting in more pronounced reflections. The increasing depth allows the structure to interact with a greater portion of the wave's energy, amplifying the reflection. In panels with H_i/L = 4.99×10^{-2} (higher steepness), the reflection is more intense and well-defined, reflecting the higher energy content of steeper waves. In contrast, H_i/L = 9.7×10^{-3} (lower steepness) cases show milder reflections, as less energy is available for reflection.

Figure 6 presents time-series data comparing H_{max} and H_{min} for two wave steepness values (H_i/L = 0.04995 and H_i/L = 0.0097) across different h/d. H_{max} was measured at WP1, while H_{min} was measured at WP2. The plots show that as h/d increases, both H_{max} and H_{min} stabilize over time after interacting with the

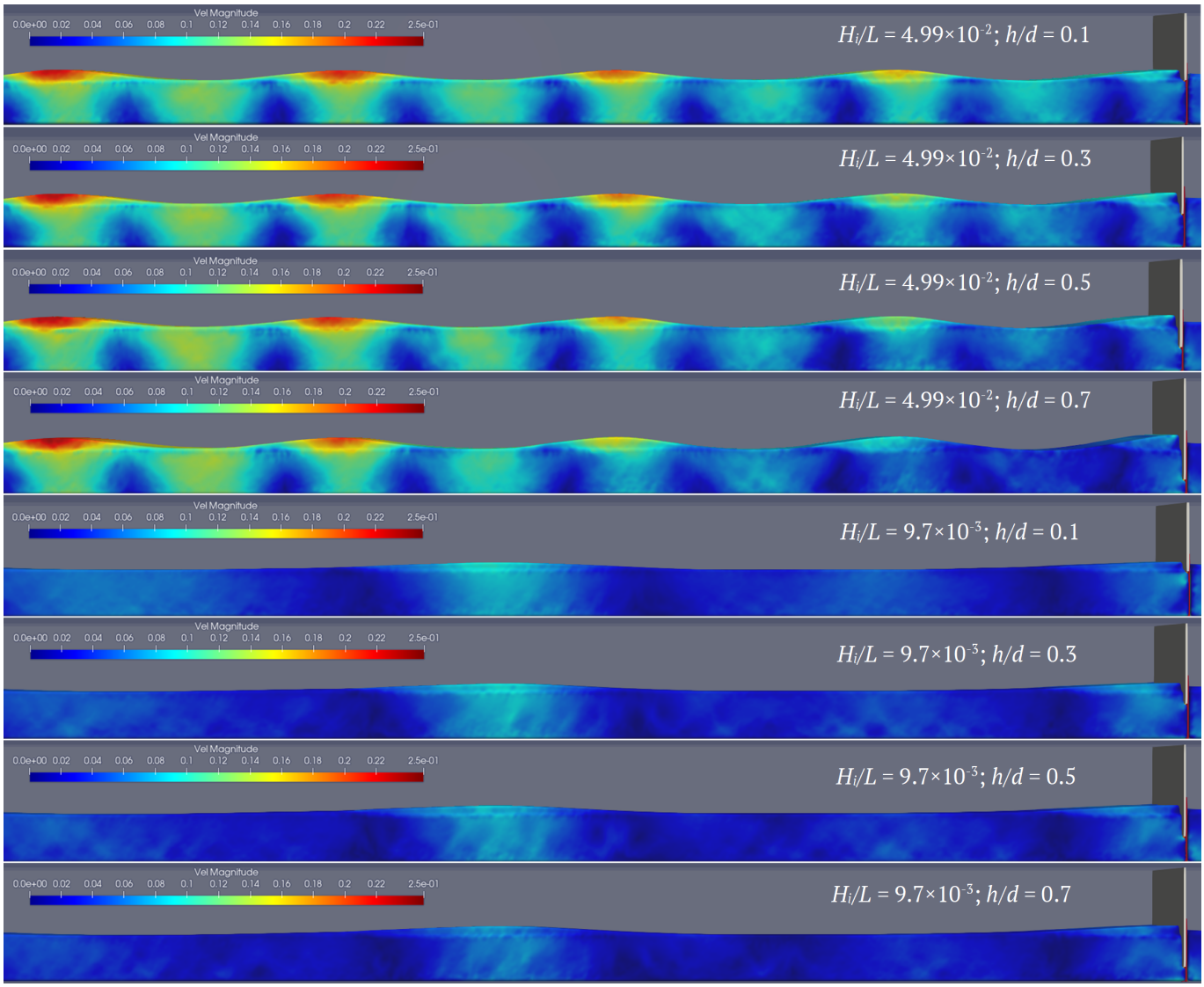

Figure 5 Simulation visualization of wave reflection patterns for varying wave steepness (H_i/L) and relative depth (h/d).

structure, with deeper breakwater walls resulting in more pronounced and steady wave patterns. The plots also highlight that higher wave steepness leads to greater variations in wave amplitudes, reflecting the breakwater's increased effectiveness in modifying wave behavior. In the context of breakwater design and wave mechanics, the relationship between wave steepness and relative depth is crucial for understanding wave pattern and stability. Wave steepness provides insight into the wave's potential for breaking or interacting with coastal structures. Relative depth influences how waves propagate and transform as they are reflected by the breakwater. Furthermore, as h/d increases, H_{max} generally rises, and H_{min} generally decreases. Specifically, H_{max} increases, indicating that a greater relative depth results in higher maximum water elevations. Meanwhile, H_{min} decreases, suggesting that the minimum water elevation reduces with increasing relative depth. Lower wave steepness exhibits similar trends, but with lower overall values than in higher wave steepness. These findings imply that a deeper breakwater wall can obstruct more water and lead to higher waves while also reducing the node fluctuations of waves. The linear trend lines provide a simplified representation of this relationship, useful for predicting water elevation behavior.

Table 3 complements these observations by showing specific numerical values. For H_i/L = 0.0097, H_{max} increases from 26.179 mm at h/d = 0 to 37.588 mm at h/d = 0.7, while H_{min} decreases from 18.736 mm to 11.182 mm over the same range. Similarly, for H_i/L = 0.04995, H_{max} increases from 57.458 mm at h/d = 0

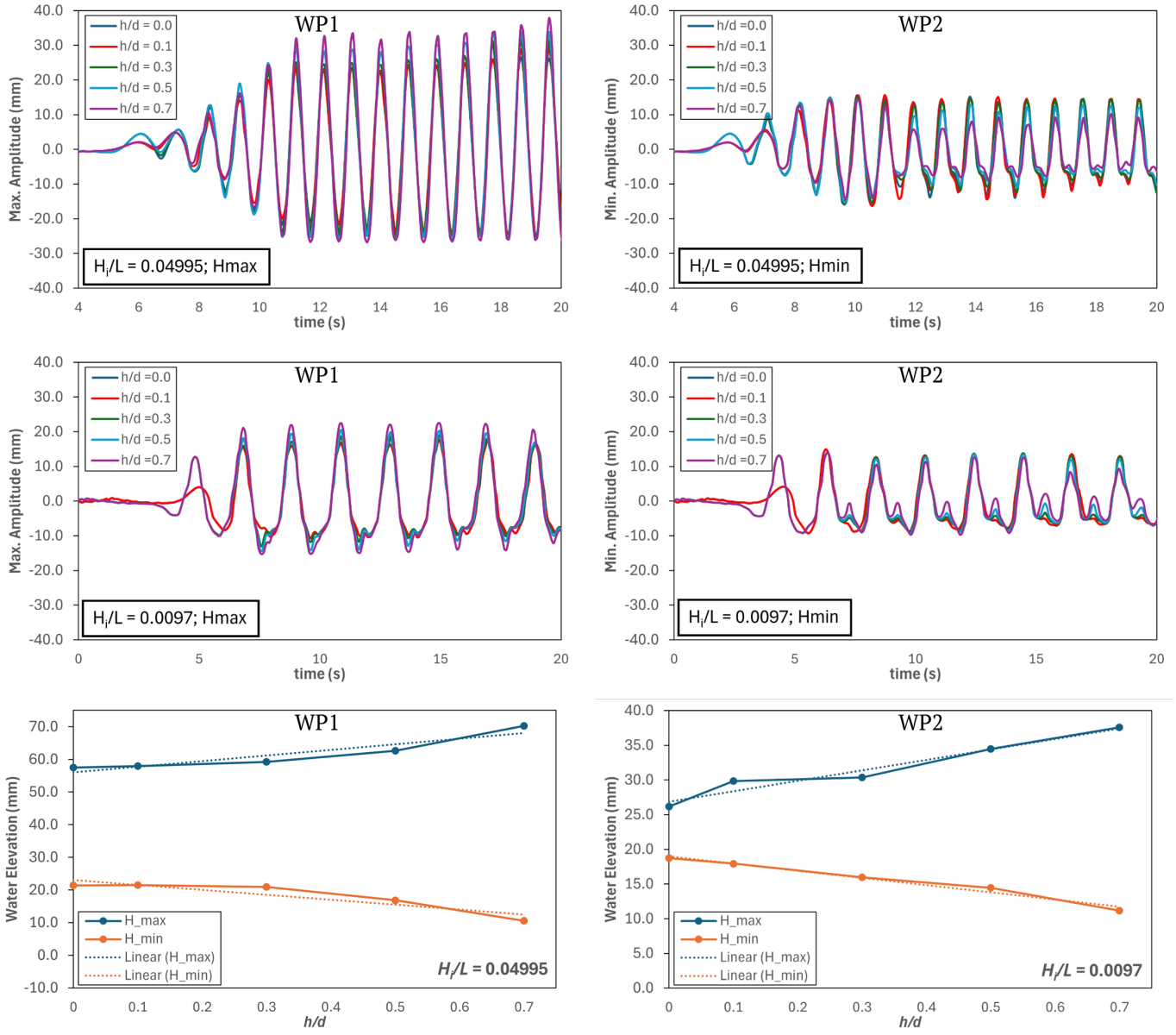

Figure 6 Maximum and minimum wave elevation as a function of h/d. The plot also shows H_{max} and H_{min} with linear trend lines, indicating how wave heights vary with changes in h/d for both H_i/L values.

Table 3. Maximum and minimum wave elevations for different wave periods and breakwater's relative water depths.

	H_i/L	h/d				
		0	0.1	0.3	0.5	0.7
H_{max} (mm)	0.0097	26.179	29.824	30.364	34.46	37.588
H_{min} (mm)		18.736	17.927	15.967	14.461	11.182
H_{max} (mm)	0.0499	57.458	57.953	59.218	62.602	70.226
H_{min} (mm)		21.404	21.446	20.915	16.849	10.556

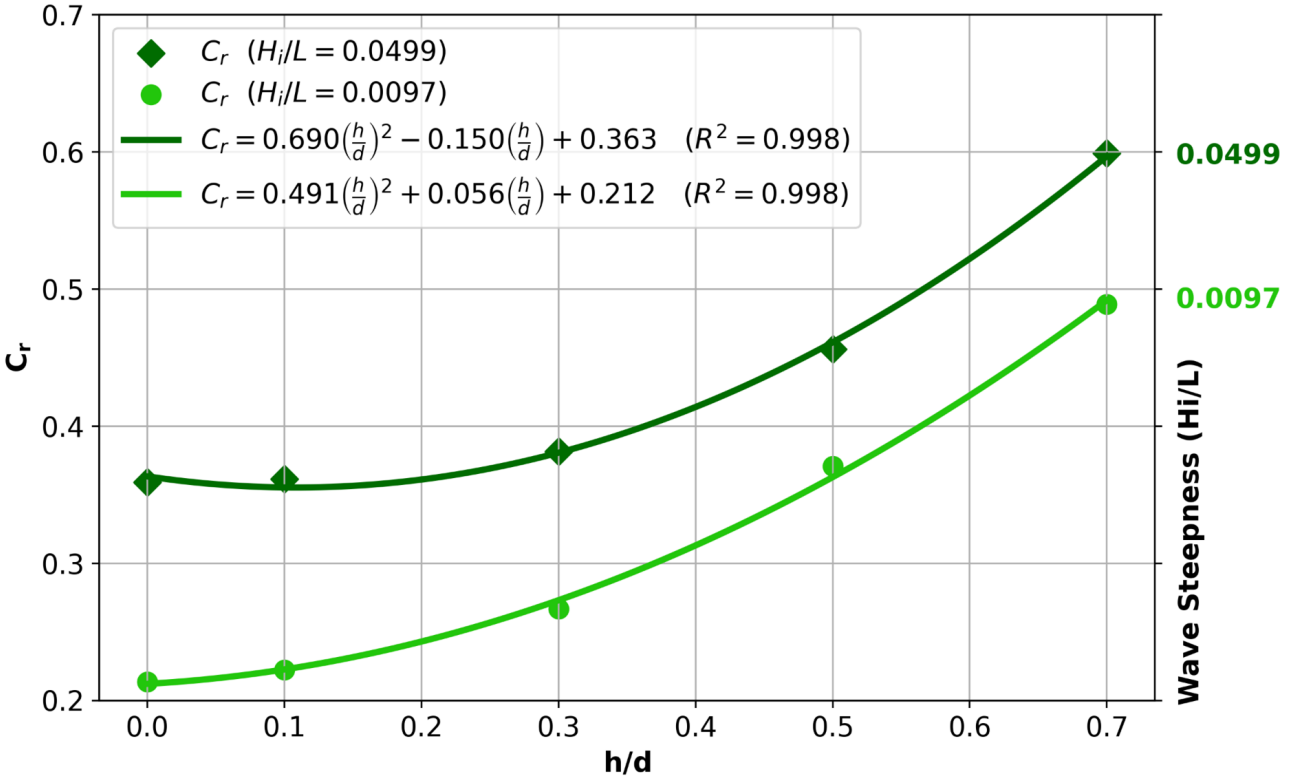

Figure 7 Quadratic correlation between the breakwater's relative depth on the reflection coefficient for two wave steepness values. The results indicate an increasing trend in C_r with h/d and H_i/L.

to 70.226 mm at h/d = 0.7, and H_{min} decreases from 21.404 mm to 10.556 mm. These detailed observations show that varying the relative depth of the breakwater significantly influences wave characteristics, with higher H_{max} values indicating greater wave heights and lower H_{min} values indicating reduced wave node fluctuations in partially standing waves

The correlation between C_r and h/d can be explained using empirical or semi-empirical regression equations obtained from numerical investigations. These equations generally demonstrate a quadratic correlation, indicating that the value of C_r increases as h/d increases. Figure 7 illustrates the relationship between h/d and C_r for two different wave steepness values (H_i/L = 0.0499 and H_i/L = 0.0097). The x-axis represents h/d, while the y-axis shows C_r. The data points are fitted with quadratic regression lines, demonstrating the strong correlation between these variables, as indicated by the high R^2 values of 0.998 for both wave steepness scenarios. For H_i/L = 0.0499, the C_r starts at approximately 0.36 for h/d = 0 and increases to around 0.60 for h/d = 0.7. The quadratic regression equation for this wave steepness is $C_r = 0.69\left(\frac{h}{d}\right)^2 - 0.150\left(\frac{h}{d}\right) + 0.363$. It is suggesting that the reflection coefficient rises significantly with increasing relative depth. This indicates that deeper breakwaters are more effective at reflecting wave energy, which is critical for reducing wave impacts on the protected side.

Similarly, for H_i/L = 0.0097, C_r starts lower at approximately 0.21 for h/d = 0 and increases to about 0.49 for h/d = 0.7. The corresponding quadratic regression equation is $C_r = 0.491\left(\frac{h}{d}\right)^2 + 0.056\left(\frac{h}{d}\right) + 0.212$, which also shows a substantial increase in the reflection coefficient with increasing relative depth, although less significant than for the higher wave steepness.

Furthermore, the analysis highlights that wave steepness significantly influences the effectiveness of a breakwater as well as the relative depth. Higher wave steepness results in a greater reflection coefficient for the same relative depth compared to lower wave steepness. This indicates that steeper waves, which have a higher energy concentration and impact force, are more effectively reflected by the breakwater structure. The higher reflection coefficient associated with steeper waves suggests that the breakwater can more efficiently deflect the wave energy, reducing the energy transmitted past the structure.

4 CONCLUSION

The effectiveness of the CPB was extensively evaluated through numerical simulations using the SPH model, implemented via DualSPHysics. The choice of a 0.5 cm particle size was made to balance computational efficiency with the need for detailed resolution. While smaller particle sizes can provide even more detail, they also significantly increase computational demands. The selected particle size of 0.5 cm was determined to be optimal for capturing the necessary physical details without incurring prohibitive computational costs. The results confirmed that the CPB's design significantly influences its performance in wave reflection, primarily governed by the ratio of the wall depth to the water depth and the wave steepness. Specifically, as h/d increased from 0.0 to 0.7 resulted in an increase in C_r from approximately 0.21 to 0.49 for low wave steepness (H_i/L = 0.0097), and from approximately 0.36 to 0.60 for high wave steepness (H_i/L = 0.0499). Higher H_i/L results in a greater C_r for the same relative depth compared to lower H_i/L. For instance, at h/d = 0.5, C_r was approximately 0.46 for higher H_i/L and 0.37 for lower H_i/L. This indicates a sensitivity of the reflection coefficient to wave steepness as well, necessitating robust breakwater designs to address different wave conditions effectively. These findings highlight the importance of considering both wall depth and wave steepness in breakwater design. Future work could expand on these findings by exploring the impact of other variables such as pile configuration, pile dimension and wall material properties, further refining the design guidelines for CPB structures.

DISCLAIMER

The authors declare no conflict of interest.

ACKNOWLEDGMENTS

The authors would like to express sincere gratitude to the Hydraulic Laboratory at PAU Universitas Gadjah Mada for providing the facilities and support necessary to conduct the experimental part of this research. The use of their wave flume and other laboratory resources was instrumental in validating the numerical simulations and ensuring the accuracy of our findings.

REFERENCES

Aghaei, B., Arasteh, A., Lari, K. and Torabi Azad, M. (2021), 'Numerical modeling of wave reflection from sloped impermeable seawalls using the sph method: Case study of chabahar port', *Advances in Civil Engineering* .
URL: *https://doi.org/10.1155/2021/7382416*

Altomare, C., Crespo, A., Domínguez, J., Gómez-Gesteira, M., Suzuki, T. and Verwaest, T. (2015), 'Applicability of smoothed particle hydrodynamics for estimation of sea wave impact on coastal structures', *Coastal Engineering* **96**, 1–12.
URL: *https://doi.org/10.1016/j.coastaleng.2014.11.001.*

Barreiro, A., Crespo, A., Domínguez, J. and Gómez-Gesteira, M. (2013), 'Smoothed particle hydrodynamics for coastal engineering problems', *Computers and Structures* **120**, 96–106.
URL: *https://doi.org/10.1016/j.compstruc.2013.02.010*

Batchelor, G. (1999), *An introduction to fluid dynamics*, Cambridge University Press.

Crespo, A., Domínguez, J., Rogers, B., Gómez-Gesteira, M., Longshaw, S., Canelas, R., Vacondio, R., Barreiro, A. and García-Feal, O. (2015), 'Dualsphysics: Open-source parallel cfd solver based on smoothed particle hydrodynamics (sph)', *Computer Physics Communications* **187**, 204–216.
URL: *https://doi.org/10.1016/j.cpc.2014.10.004*

Dean, R. and A, D. R. (1984), *WATER WAVE MECHANICS FOR ENGINEERS AND SCIENTISTS*, Prentice Hall.

Domínguez, J., Fourtakas, G., Altomare, C., Canelas, R., Tafuni, A., García-Feal, O., Martínez-Estévez, I., Mokos, A., Vacondio, R., Crespo, A., Rogers, B., Stansby, P. and Gómez-Gesteira, M. (2021), 'Dualsphysics: from fluid dynamics to multiphysics problems', *Computational Particle Mechanics* **9**, 867–895.
URL: *https://doi.org/10.1007/s40571-021-00404-2*

Fourtakas, G. and Rogers, B. (2016), 'Modelling multi-phase liquid-sediment scour and resuspension induced by rapid flows using smoothed particle hydrodynamics (sph) accelerated with a graphics processing unit (gpu)', *Advances in Water Resources* **92**, 186–199.
URL: *https://doi.org/10.1016/j.advwatres.2016.04.009*

Khaldirian, M., Rahardjo, A., Luknanto, D. and Sondi, R. (2021), 'An alternative algorithm for simulating flash flood', *IOP Conference Series: Earth and Environmental*

Science .
URL: *https://doi.org/10.1088/1755-1315/930/1/012076*

Laju, K., Sundar, V., Sundaravadivelu, R. and Scholar, R. (2005), 'Studies on pile supported skirt breakwater'.

Luo, M., Khayyer, A. and Lin, P. (2021), 'Particle methods in ocean and coastal engineering', *Applied Ocean Research* **114**.
URL: *https://doi.org/10.1016/j.apor.2021.102734*

Madsen, O. (1971), 'On the generation of long waves', *Journal of Geophysical Research* **76**(36), 8672–8683.

Monaghan, J. (1994), 'Simulating free surface flows with sph', *Journal of Computational Physics* **110**(2), 399–406.
URL: *https://doi.org/10.1006/jcph.1994.1034*

Pawitan, K., Garlock, M. and Wang, S. (2024), 'Multiphase sph analysis of a breaking wave impact on elevated structures with vertical and inclined walls', *Applied Ocean Research* **142**.
URL: *https://doi.org/10.1016/j.apor.2023.103832*

Rao, N., Suryanarayana Barimar Rao, P., Nayak, K., Kishor Pal, S., Hunasanahally Sathyanarayana, A., Suvarna, P. and Umesh, P. (2019), 'Numerical investigation on wave transmission characteristics of perforated and non-perforated pile breakwater', *Journal of Physics: Conference Series. Institute of Physics Publishing* .
URL: *https://doi.org/10.1088/1742-6596/1276/1/012021*

Reis, C., Barbosa, A., Figueiredo, J., Clain, S., Lopes, M. and Baptista, M. (2022), 'Smoothed particle hydrodynamics modeling of elevated structures impacted by tsunami-like waves', *Engineering Structures* **270**.
URL: *https://doi.org/10.1016/j.engstruct.2022.114851*

Subekti, S. and Shulhany, A. (2021), 'Transmission and reflection of waves on curtain wall breakwater', *Teknika: Jurnal Sains dan Teknologi* **17**(1), 100.
URL: *https://doi.org/10.36055/tjst.v17i1.11026*

Suh, K.-D., Asce, A., Shin, S., Asce, S., Cox, D. and Asce, M. (2006), 'Hydrodynamic characteristics of pile-supported vertical wall breakwaters', *Journal of Waterway, Port, Coastal, and Ocean Engineering* **132**(2), 83–96.
URL: *https://doi.org/10.1061/(ASCE)0733-950X(2006)132:2(83)*

Suh, K., Jung, H. and Pyun, C. (2007), 'Wave reflection and transmission by curtainwall-pile breakwaters using circular piles', *Ocean Engineering* **34**(14-15), 2100–2106.
URL: *https://doi.org/10.1016/j.oceaneng.2007.02.007*

Tahalele, M., Triatmadja, R. and Yuwono, N. (2022), 'Aliran pada lubang gerusan: Model fisik dan model numerik flow in the scouring hole: Physical and numerical models', *Journal of Water Resources Engineering* **13**(2), 258–272.
URL: *https://doi.org/10.21776/ub.pengairan.2022.013.02.11*

Vu, H., Zemann, M., Oberle, P., Seidel, F. and Nestmann, F. (2022), 'Investigating wave transmission through curtain wall breakwaters under variable conditions', *Journal of Coastal and Hydraulic Structures* **2**.
URL: *https://doi.org/10.48438/jchs.2022.0019*

Wendland, H. (1995), 'Piecewise polynomial, positive definite and compactly supported radial functions of minimal degree', *Advances in Computational Mathematics* **4**(1), 389–396.
URL: *https://doi.org/10.1007/BF02123482*

Wibowo, A., Ajiwibowo, H., Wurjanto, A. and Ghani, A. (2020), 'Two-dimensional physical modeling of single chamber skirt breakwater (scsb)', *International Journal of GEOMATE* **19**(74), 83–90.
URL: *https://doi.org/10.21660/2020.74.53146*